Origin of the metal-insulator transition in ultrathin films of $La_{2/3}Sr_{1/3}MnO_3$

Zhaoliang Liao,[1] Fengmiao Li,[2] Peng Gao,[3] Lin Li,[2] Jiandong Guo,[2] Xiaoqing Pan,[3] R. Jin,[1] E. W. Plummer,[1] and Jiandi Zhang[1,*]

[1]*Department of Physics and Astronomy, Louisiana State University, Baton Rouge, Louisiana 70803, USA*

[2]*Beijing National Laboratory for Condensed Matter Physics and Institute of Physics, Chinese Academy of Sciences, Beijing 100190, China*

[3]*Department of Materials Science and Engineering, University of Michigan, Ann Arbor, Michigan 48109, USA*

(Received 22 June 2015; published 14 September 2015; publisher error corrected 18 September 2015)

Many ultrathin films of transition metal oxides exhibit nonmetallic behavior, in contrast to their metallic bulk counterpart, thus displaying a metal-insulator transition (MIT) as the film thickness is reduced. The nature of this MIT has been a long-standing issue in the epitaxial oxide research community. Here, we report the processing dependence of the critical thickness (t_c) of MIT and the origin of the insulating phase in $La_{2/3}Sr_{1/3}MnO_3$ (LSMO) films. A t_c of 3 unit cells (u.c.) is achieved by minimizing oxygen vacancies under optimal growth conditions, diminishing the epitaxial strain with a tunable buffer layer and suppressing surface strain by film capping. The electrical transport measurements demonstrate that the nonmetallic behavior in LSMO thin films is an unavoidable result of localization initiated by inherent disorder but amplified by the reduction in dimensionality.

DOI: 10.1103/PhysRevB.92.125123 PACS number(s): 71.30.+h, 71.27.+a, 73.20.Fz, 73.50.−h

Tailoring complex oxides for new functionality by artificial growth with atomic precision is a forefront area of research in condensed matter physics [1]. By introducing surface [2], interface [3], strain [4], and reduced dimensionality [5,6], interesting physical properties emerge, which can be fundamentally different from those exhibited in their corresponding bulk forms. The interface between two insulating oxides, such as $LaAlO_3$ (LAO)/$SrTiO_3$ (STO), exhibits two-dimensional (2D) electron gas [7] and superconductivity [8]. In contrast, many films of metallic oxides, such as $SrVO_3$ [5], $LaNiO_3$ [9,10], $SrRuO_3$ [11], and $La_{1-x}Sr_xMnO_3$ [12–18], become nonmetallic in the ground state below a critical thickness (t_c), thus referred to as "dead" layer behavior. Despite extensive research, the nature of such a thickness-driven metal-insulator transition (MIT) remains mysterious. In addition to an intrinsic driving force for the transition, extrinsic factors, such as film crystallinity and oxygen stoichiometry, also play vital roles in the transition [10,19]. How to avoid or minimize extrinsic effects and gain insight into the nature of the transition is the goal of this paper.

$La_{2/3}Sr_{1/3}MnO_3$ (LSMO) is an attractive material for both fundamental physics concepts and potential technological application because it is spin polarized and the most itinerant electron material with the highest Curie temperature ($T_C \approx 369$ K) among manganites [20]. However, the spin-polarized and metallic (referred to as half-metal) character disappears as the material is prepared in the thin film form. The (001) oriented LSMO thin films become insulating below a critical thickness, which depends on substrates and growth conditions [12–18]. Interface electronic reconstruction [17,21], such as orbital ordering, has been proposed to explain such a thickness-induced MIT. For example, Tebano *et al.* [17] and Lepetit *et al.* [21] showed that the LSMO films grown on STO (001) substrates exhibit $d_{3z^2-r^2}$ orbital ordering at the interface, thus resulting in nonmetallic behavior in the ultrathin films. However, Huijben *et al.* revealed that there is no formation of such $d_{3z^2-r^2}$ orbital ordering, even in ultrathin films down to 3 unit cells (u.c.) thick [16]. Inconsistent values for the critical thickness (t_c), such as 4.0 nm [14], 3.0 nm [16], and 2.7 nm [17] on STO (001), have been reported by different groups. Such inconsistence indicates that there must be some extrinsic effects involving in, such as structure imperfection [19] and oxygen deficiency [22]. The reported values of t_c for doped oxide films such as LSMO are also larger than the critical thickness of several undoped metallic oxide films, such as $LaNiO_3$, $SrVO_3$, and $SrRuO_3$ [5,9–11], suggesting that the chemical inhomogeneity or *A*-site disorder in LSMO may enhance carrier localization and result in a larger t_c.

In this paper, we report a systematic evaluation of critical thickness t_c for the MIT of LSMO by minimizing oxygen vacancies and engineering strain and interface. The minimum t_c of 3 u.c. for the MIT transition is achieved for STO-sandwiched LSMO films by diminishing the substrate-induced strain and surface effects. Through the analysis of low temperature (T) electrical transport property and density functional theory (DFT) calculations, we conclude that the existence of finite experimental minimum t_c can be attributed to the localization effect that is induced probably by oxygen vacancies and/or *A*-site cation disorder. As film thickness is reduced, the effect of individual vacancy as a defect enhances. Such unavoidable localization serves as the universal "driving force" for the MIT in many ultrathin oxide films.

Figure 1(a) illustrates the lattice structure of ultrathin LSMO films epitaxially grown on STO (001), a widely used ABO_3 perovskite substrate. The LSMO films were grown by ultrahigh vacuum-pulsed laser deposition. A KrF excimer laser ($\lambda = 248$ nm) at a repetition rate of 3 Hz and a laser flounce of $\sim 1\,J/cm^2$ was used. TiO_2-terminated STO (001) substrates [23] were used. To obtain an oxygen stoichiometry film, a strongly oxidant background gas ($O_2 + 2$ wt% O_3) was utilized. During growth, the substrates were maintained at 700 °C. With this condition, a universal layer-by-layer growth was achieved for different oxidant gas partial pressure (P_O), ranging from 10^{-6} Torr to 180 mTorr. The atomically flat LSMO surface and sharp interface between LSMO/STO were achieved as characterized in the images with both scanning tunneling microscopy (STM) and scanning transmission

*jiandiz@lsu.edu

 ©2015 American Physical Society

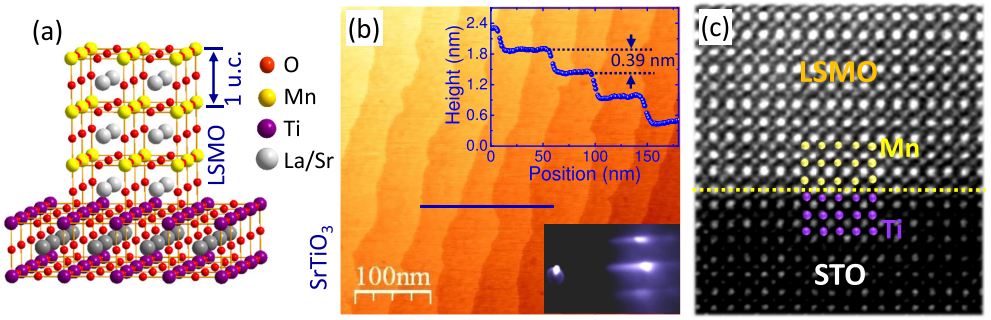

FIG. 1. (Color online) Atomic layer-by-layer growth of LSMO on STO (001): (a) schematic structure model of a 3 u.c. LSMO on the perovskite substrate. (b) Surface morphology of a 10 u.c. LSMO thin film on Nb-doped STO imaged by STM ($V_{tip} = 2$ V, $I_t = 300$ pA). Inset shows the profile along the blue line. (c) Cross-section STEM image of the LSMO/STO. The film was grown at $P_O = 80$ mTorr.

electron microscopy (STEM, JOEL 2100F), shown in Figs. 1(b) and 1(c). There is no obvious structure defect in our STEM cross-section image [see Fig. 1(c)] within the LSMO film and at the interface. The step height, as shown in Fig. 1(b), is ~0.39 nm, which equals 1 u.c. thickness. This indicates that the surface layer is identical. A 2D flat surface is also indicated by the reflection high-energy electron diffraction (RHEED) pattern in the inset of Fig. 1(b). The surface topography of all films was also characterized by the RHEED patterns indicating 2D surfaces.

The oxygen stoichiometry was optimized by investigating the effect of oxygen partial pressure (P_O) on the electrical and magnetic properties, which were measured by the Physical Property Measurement System (PPMS) and Quantum Design superconducting quantum interference device (SQUID), respectively. The resistivity was measured by a standard four probe method. Figure 2(a) shows the T dependence of resistivity (ρ) of LSMO films grown at P_O of 130 mTorr for different film thickness. For thick films, $\rho(T)$ exhibits MIT with increasing temperature, similar to that in the bulk. However, the transition temperature (T_{MIT}), which is defined by the peak position at the $d\rho/dT$ curve, decreases dramatically with decreasing film thickness. When the LSMO film is equal to or less than 6 u.c., the ground state of films becomes insulating rather than metallic as seen in the thick films and bulk. Thus, the critical thickness $t_c = 6$ u.c. is obtained for the films grown at $P_O = 130$ mTorr.

The critical thickness apparently varies with oxygen partial pressure. Figure 2(b) summarizes the thickness dependence of T_{MIT} of the films grown at different P_O (from 1 μTorr to

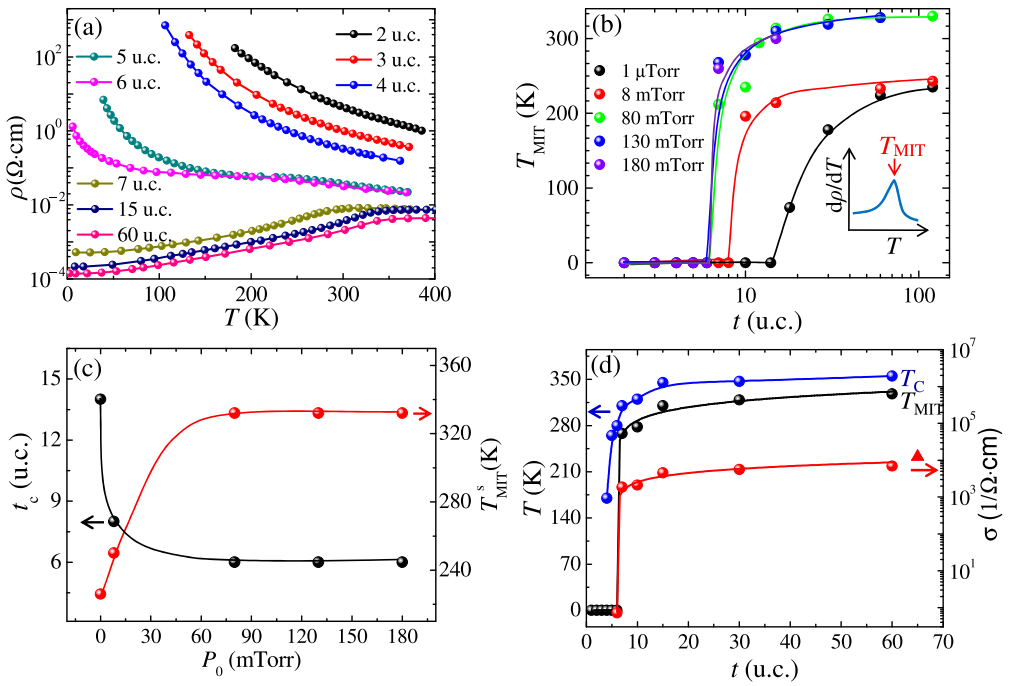

FIG. 2. (Color online) (a) The T dependence of resistivity of LSMO films grown on STO(001) at oxygen pressure $P_O = 130$ mTorr for different thickness. (b) Thickness dependence of T_{MIT} for the LSMO films grown at different P_O. The T_{MIT} is determined by the maximum of the first derivative of resistivity versus temperature (see inset). (c) P_O dependence of the critical thickness (t_c) for MIT and the saturated T_{MIT} (T^S_{MIT}) of LSMO films. (d) Thickness dependence of Curie temperature T_C (blue), T_{MIT} (black), and conductivity σ at 6 K (red) of the LSMO films grown at $P_O = 130$ mTorr.

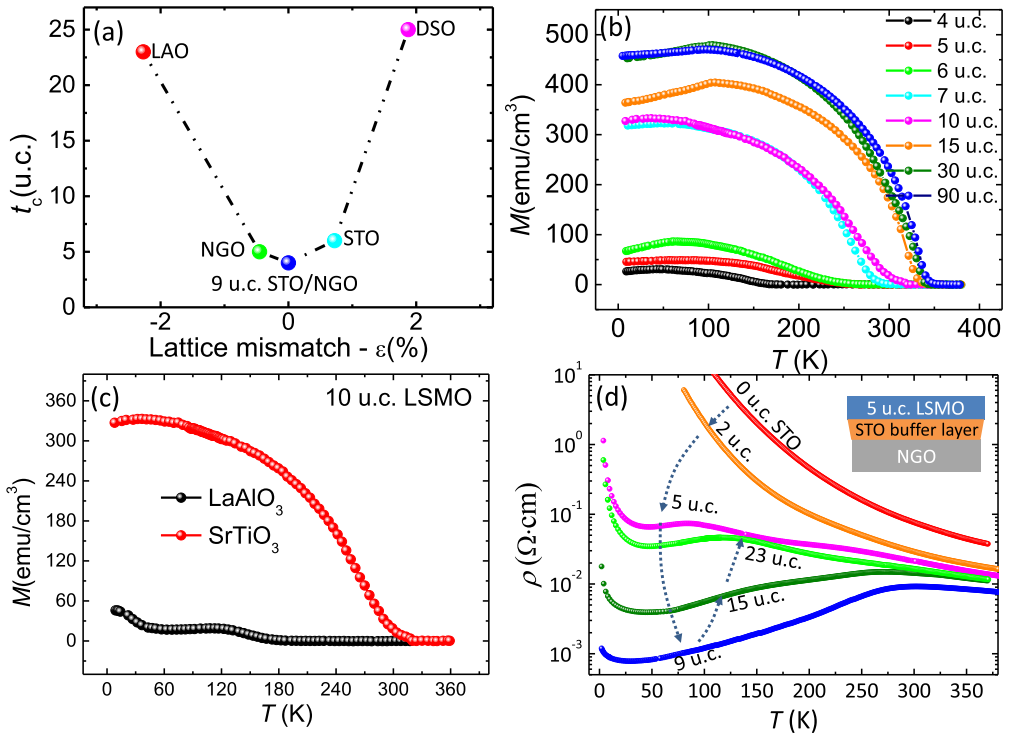

FIG. 3. (Color online) (a) Substrate-induced strain dependence of the critical thickness (t_c) for MIT in LSMO films. (b) T-dependent magnetization of different thickness of LSMO films on STO(001). (c) The T-dependent magnetization of 10 u.c. LSMO film on LAO and STO substrates. All samples were field cooled at 1 T from 360 to 2 K along in-plane [100] before measurement, and the magnetization was measured at 150 Oe on warming. (d) Resistivity for a 5 u.c. LSMO film on NGO (110) substrate as a function of STO buffer layer thickness (see the inset for a schematic side view of film arrangement).

180 mTorr). Thus, t_c is defined as the onset of the T_{MIT} for a given P_O. Note that t_c decreases and the saturated T_{MIT} (T^S_{MIT}, which is defined as the saturated value with film thickness) increases with increasing P_O until $P_O \geqslant 80$ mTorr, indicating strong dependence on oxygen composition. To identify the saturated P_O for minimizing oxygen deficiency, we plot t_c and T^S_{MIT} as a function of P_O in Fig. 2(c), respectively. As $P_O \geqslant 80$ mTorr, which is referred to as the optimized pressure for the growth, the minimum value of t_c (6 u.c.) is achieved.

There is a crossover thickness range above t_c before the film fully develops into bulklike properties [24], even grown under the optimized oxygen partial pressure. As shown in Fig. 2(d), for the films grown at $P_O = 130$ mTorr, T_{MIT}, Curie temperature (T_C) (determined from magnetization measurements) and the electrical conductivity $\sigma(\sigma = 1/\rho)$ measured at 6 K increase with increasing thickness and then saturate around 15 u.c. at the values almost equal to these of the bulk [24]. The existence of such a crossover thickness range (from $t_c = 6$ u.c. to ~15 u.c.) indicates a gradual evolution of the film toward the bulk. Because of the difference in chemical composition [25] and lattice structure [26], the physical properties near surface and the interface cannot be the same as the inside of the film. This will result in a difference in overall film property from the bulk, especially when film is not thick enough. In contrast to the sharp onsets of T_{MIT} and electrical conductivity, T_C shows a gradual change across t_c. As shown in Fig. 2(d), the 4 and 5 u.c. LSMO films on STO (001) are nonmetallic but exhibit ferromagnetism with T_C of 170 and 265 K, respectively. Such decoupled magnetism and transport behavior in ultrathin films may be related to the localization effects that are important and will be discussed later.

After optimizing P_O, we are able to further investigate the substrate-induced strain effect on t_c. We have grown LSMO films on the substrates with different lattice constants under constant $P_O = 130$ mTorr. A layer-by-layer growth mode was observed for film growth on these substrates. Figure 3(a) presents the dependence of the critical thickness on the lattice mismatch of different substrates to the bulk of LSMO ($a_{LSMO} = 3.88$ Å) under a pseudocubic perovskite structure. It is obvious that any substrate-induced strain as quantified by the lattice mismatch ($\varepsilon = \frac{a_{sub} - a_{LSMO}}{a_{LSMO}} \times 100\%$), either compressive, such as from LAO (001), or a tensile one from $DyScO_3$ (DSO) (110), results in a significant increase of t_c. With the smallest lattice mismatch $\varepsilon = -0.5\%$ for the film on $NdGaO_3$ (NGO) (110), t_c decreases to 5 u.c. Therefore, it is expected that the minimum t_c is achieved for a strain-free film.

The thickness and strain effects on magnetization were investigated in an attempt to determine the origin of dead layer. The temperature dependent magnetization for different thickness of LSMO films on STO is shown in Fig. 3(b). It is clear that the ferromagnetism is greatly suppressed with reducing thickness but still survives in ultrathin films (even below t_c), consistent with previous report from Huijben *et al.* [16]. Therefore, there is clearly decoupling between ferromagnetism and transport. The T_C for 6 u.c. LSMO/STO is still as high as ~280 K. The decoupling of metallicity with ferromagnetism [16] indicates that the electric dead layer is not magnetic in origin.

Substrate strain dramatically affects the magnetic property in ultrathin LSMO films. A relatively thick 10 u.c. LSMO film on LAO shows a significant weaker magnetization than that on STO [see Fig. 3(c)]. The strong suppression in magnetization of LSMO/LAO is due to the large compressive strain induced by the LAO substrate, which enhances antiferromagnetism in LSMO by suppressing the double-exchange interactions [16,17]. A compressed strain, which elongates the MnO_6 octahedron, promotes the $e_g - d_{3z^2-r^2}$ occupancy and thus favors *C*-type anti-ferromagnetic (AFM) ordering.

To achieve the strain-free or the minimum strain condition on LSMO films, we use a strained STO buffer layer grown on the NGO (110) substrate before growing LSMO films. Realizing the sequence of the lattice constant of these three materials, $a_{NGO} < a_{LSMO} < a_{STO}$, we are able to tune a proper thickness of STO buffer layer so that the surface lattice constant of STO layer relaxes toward a_{LSMO} from a_{NGO} of the substrate. Figure 3(d) shows the resistivity of 5 u.c. LSMO film grown on the different thicknesses of the STO buffer layers on the NGO (110) substrate. While the 5 u.c. LSMO film on NGO (110) is insulating, the introduction of STO buffer layer induces an insulator to metal transition when the buffer layer is thicker than 5 u.c. The transition temperature T_{MIT} increases with increasing the buffer layer thickness from 5 to 9 u.c., and then decreases above 9 u.c. Such nonmonotonic variation of T_{MIT} on the LSMO film with STO buffer layer thickness can be understood by the change of lattice strain (or ε). Though there is no data on the lattice constant in the strained STO buffer layer as a function of thickness, our data imply that the 9 u.c. STO buffer layer on NGO results in the best lattice match (i.e., close to zero lattice mismatch) to LSMO films and thus is able to convert the 5 u.c. LSMO film to a metallic ground state. The optimized T_{MIT} of the 5 u.c. LSMO film on 9 u.c. STO buffer layer reaches ~252 K. Similar to that shown in Fig. 2(b), T_{MIT} quickly drops to zero when thickness is reduced to 4 u.c., indicating $t_c = 4$ u.c. in this case.

Strain leads to the enhancement of nonmetallic behavior of LSMO. The tensile strain causes the flattering of MnO_6 octahedron, and the e_g electron prefers to occupy $d_{x^2-y^2}$ orbital [16,17,27,28], thus driving the system to be in an *A*-type AFM insulating state. The compressed strain, on the other hand, elongates MnO_6 octahedron resulting in $d_{3z^2-r^2}$ orbital ordering that favors the *C*-type AFM insulating phase. Now, a question is the following: what is the origin of the finite t_c, even for a strain-free LSMO film? In an attempt to answer the question, we have performed first-principles calculations to study the electronic structure of single monolayer LSMO on STO substrate by using the DFT plus on-site Coulomb interaction (DFT + U) approach. The results are displayed in Fig. 4. The calculations were carried out using the Vienna *Ab initio* Simulation Package (VASP) code [29]. We used the projector augmented-wave method [30] and the Perdew-Burke-Ernzerhof functional [31] with kinetic energy 400 eV. The Hubbard U acting on the Ti and Mn 3d states are $U_{Ti} = 8.0$ eV and $U_{Mn} = 2.0$ eV, respectively. The DFT + U calculation reproduces the ferromagnetic and half-metal properties in bulk LSMO [24,32]. To model the LSMO/STO interface, we adopt the (3 × 1) slab model, as shown in Fig. 4(a), with inversion symmetry along the direction normal to the film

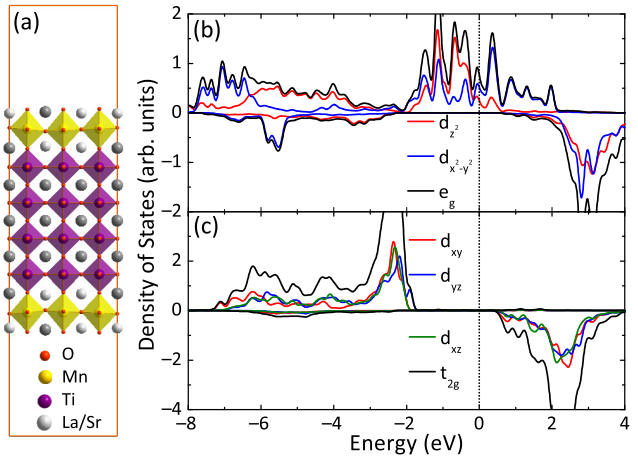

FIG. 4. (Color online) (a) The optimized slab model of a single unit cell thickness of LSMO film on STO(001) for the DFT + U ($U_{Mn} = 2.0$ eV and $U_{Ti} = 8.0$ eV) calculations. The calculated orbital- and spin-resolved densities of states for both (b) e_g and (c) t_{2g} orbitals. The single layer LSMO film with ferromagnetic order is subjected to a tensile strain with in-pane lattice constant of 3.905 Å.

surface (i.e., out-of-plane direction). Only atoms in the film are relaxed along the out-of-plane direction until the force is less than 0.05 eV/Å with the (2 × 6 × 1) Monkhorst-Pack k-point mesh. We employ the (3 × 7 × 1) Monkhorst-Pack k-point mesh and 0.1 eV Gaussian smearing to plot the density of states (DOS) shown in Figs. 4(b) and 4(c). The orbital-resolved DOS of a single unit cell LSMO on STO from the DFT + U calculation is shown in Figs. 4(b) and 4(c), where there is a finite DOS at E_F and ferromagnetic ordering in the single unit cell LSMO layer, indicating that ferromagnetic metallic ground state is robust against the pure spatial confinement (thus no dead layer). Defects such as oxygen vacancies are not considered in the calculations, which could alter the electronic structure near E_F significantly in the ultrathin film case and explain the experimental observation.

We have further investigated the effect of surface strain on t_c by capping the LSMO films with crystalline STO overlayers. It is found that the STO sandwiched LSMO films exhibit a smaller t_c. With a 2 u.c. STO capping layer, the values of t_c for all the LSMO films directly grown on STO, NGO, and NGO substrates with STO buffer layer are reduced by 1 u.c. Figure 5(a) shows that 4 u.c. LSMO film grown on 9 u.c. STO buffered NGO(110) is insulating in the ground state without capping but metallic with the 2 u.c. STO capping layer. We have grown different thicknesses of LSMO films: $[(STO)_2/(LSMO)_n/(STO)_9/NGO]$ ($n = 2,3,4,5$) using both capping and buffer layers, The films show the metallic ground state when the LSMO thickness is larger than 3 u.c. ($n > 3$), as shown in Fig. 5(b), For 3 u.c. LSMO, a crossover nonmetal to metal transition can be observed at ~77 K, following a reentrance of the insulating state during cooling down. When $n = 2$, the film exhibits insulating in the whole measureable temperature range. Therefore, a minimum $t_c = 3$ u.c. is achieved by sandwiching LSMO between two STO layers on NGO substrate. The STO capping effect on t_c, which is independent on substrates, indicates that the surface also plays an important role in physical properties of films.

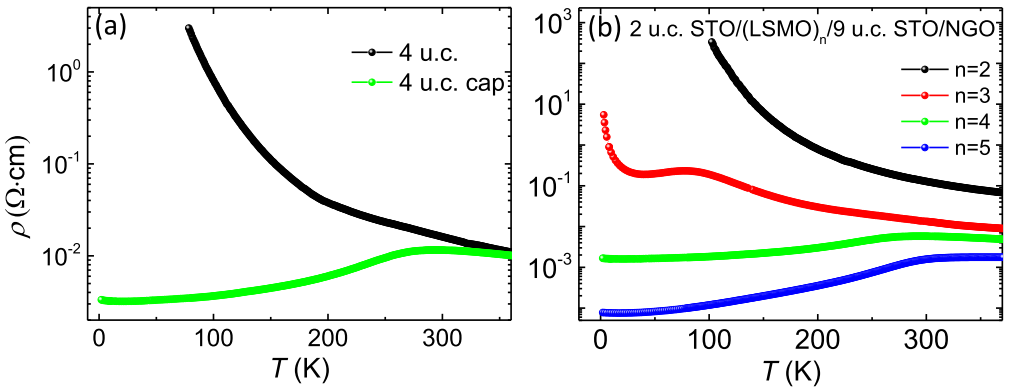

FIG. 5. (Color online) The T dependence of the resistivity for (a) 4 u.c. LSMO grown on a 9 u.c. STO buffered NGO (110) substrate with and without 2 u.c. STO capping; and (b) the different thickness of LSMO films grown on a 9 u.c. STO buffered NGO (110) substrate and capped with 2 u.c. STO capping layer.

We note that the critical thickness for both LSMO/NGO and LSMO/STO (2 u.c.)/NGO are identical, i.e., 5 u.c., while they have quite different interfaces. Therefore, the nature of substrate and capping layer does not have a strong impact on the dead layer thickness. The most likely explanation is that the STO capping layer removes the strain present at a free surface [33].

The results discussed above indicate that t_c can be reduced by proper growth procedures and by removing interface/surface strain, but t_c does not go to zero. Coupling this observation with the fact the calculations indicate that all films should be metallic, the conclusion must be that either extrinsic factors in the experiment or many-body factors left out of the theory must be considered. In fact, we will illustrate with Fig. 6 that both of these phenomena seem to be important. The unavoidable presence of oxygen vacancies and cation disorder leads to a dimensional dependence in the transport properties caused by localization. Figure 6 presents the resistance ρ

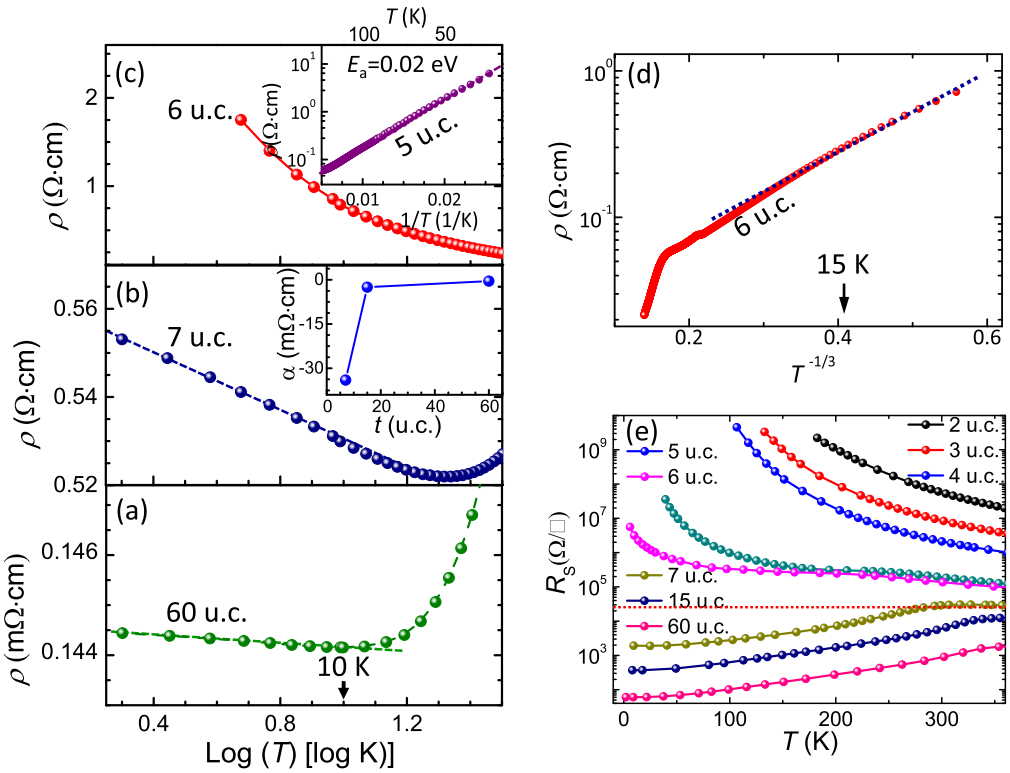

FIG. 6. (Color online) The resistivity versus $\log(T)$ for (a) 60, (b) 7, and (c) 6 u.c. LSMO films on STO (001) in low temperature range. The inset of panel (b) presents the slope (α) of resistivity versus $\log(T)$ for different film thickness and the inset of panel (c) shows the log plot of resistivity as a function of $1/T$ for 5 u.c. film, where the thermal activation energy (E_a) is extracted. (d) Log plot of resistivity as a function of $1/T^{1/3}$ for 6 u.c. LSMO/STO(001). (e) T dependence of sheet resistance for different thickness of LSMO films grown on STO(001). The red dotted line indicates the IR limit for the onset of strong localization. All the films were grown at $P_O = 130$ mTorr.

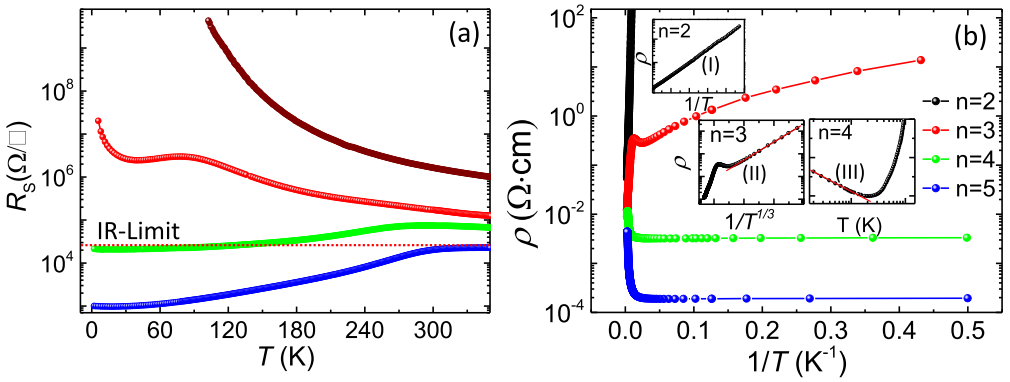

FIG. 7. (Color online) (a) T dependence of sheet resistance for different thickness of LSMO films grown on 9 u.c. STO buffered NGO with 2 u.c. STO capping layer at oxygen pressure $P_O = 130$ mTorr. The red dotted line indicates the IR limit for the onset of strong localization. (b) The corresponding log-plot of resistivity as a function of $1/T$ respectively. The inset (I) shows the low-T zoom-in plot of (I) log(ρ) versus $1/T$ for 2 u.c., (II) log(ρ) versus $1/T^{1/3}$ for 3 u.c., and (III) ρ versus log(T) for 4 u.c. film, respectively. All the films were grown at $P_O = 130$ mTorr.

versus log(T) for three different film thicknesses for LSMO grown on STO (001) [Fig. 2(a)]. The curve for the 60 u.c. thickness in Fig. 6(a) shows a slight deviation from metallic behavior at temperatures below ~10 K, which is also seen in the bulk [24]. The low temperature linear behavior of the resistivity as a function of log(T) becomes more pronounced as the film becomes thinner, as shown for 7 u.c. thicknesses in Fig. 6(b). This linear behavior is a signature of weak localization [34,35], but as the film becomes thinner, the resistivity at low temperature deviates from linear, as shown in Fig. 6(c) for 6 u.c. film. The inset in Fig. 6(b) shows the dependence of the slope of ρ versus log(T) as a function of film thickness showing a dramatic change for the films near t_c. The data indicate that what is being observed is the change in the effect of localization with dimensionality [36]. Apparently, the signature of weak localization is present down to ~7 u.c. thickness, with the 6 u.c. film showing very nonlinear behavior in the ρ vs. log(T) plot. The resistivity for 5 u.c. or thinner film displays an exponentially thermally activated behavior, as shown in the inset of Fig. 6(c). The slope of this plot gives the thermal activation energy of ~20 meV.

The film with a critical thickness of 6 u.c. LSMO on STO (001) cannot be categorized as either a thermally activated or weakly localized system. Instead, its transport behaves like a variable-range hopping (VRH) type [34,37]. The low-T resistivity exhibits linear behavior when plotted as ln(ρ) versus $T^{-1/3}$ [Fig. 6(d)], consistent with the Mott's quasi-2D VRH picture with $\rho = \rho_0 \exp(T_0/T)^{\alpha}$. Here, the exponent $\alpha = 1/3$ corresponds to a quasi-2D system [37]. This implies that there is nonzero DOS at the Fermi energy (E_F) (i.e., zero energy gap) and the transport relies on hopping [37]. The trend of low-T resistivity behavior from 7 to 5 u.c. LSMO films clearly indicates an evolution from weak localization to strong localization with reducing thickness, eventually ending with the insulating dead layer.

The transition from weak to strong localization is characterized by Ioffe-Regel (IR) limit of resistivity [34] above which the system is turned into a strong localization region. For a 2D system, the IR limit is related to sheet resistance of $R_{IR} \approx 25\,K\Omega/\square$ [9,34]. As shown in Fig. 6(e), we can find metallic films with weak localization [Figs. 6(a) and 6(b)] when the resistivity of the LSMO films on STO (001) is below IR limit, while above the IR limit, the films are nonmetallic. Similar results are observed for the STO sandwiched LSMO films on NGO (110) (2 u.c. STO/$LSMO_n$/9 u.c. STO/NGO) where a gradual weak to strong localization is observed when decreasing the thickness, as shown in Figs. 7(a) and 7(b). The IR limit separates the metallic films from insulating films [see Fig. 7(a)]. For metallic films, such as the STO sandwiched 4 u.c. film, weak localization is observed at low T [Fig. 7(b)]. With reducing thickness, the 3 u.c. film becomes strongly localized and obeys the 2D VRH transport behavior [inset panel II in Fig. 7(b)]. Further reducing the thickness below critical thickness, thermal activation is observed in the 2 u.c. LSMO [inset panel I in Fig. 7(b)]. Similar transport behavior is also observed for LSMO films with a thickness near t_c on different substrates, thus indicating a kind of universal evolution in transport with film thickness. The question to be answered by theory is, can this be explained by a dimensionality associated with Anderson localization or does the physics change as the film becomes thinner? An understanding of the dimensionality-dependent localization would have a widespread impact of interface physics.

In summary, the nature of the insulating behavior of LSMO films is systematically investigated. The epitaxial strain, oxygen vacancy, and the surface effect are found to enhance the nonmetallic behavior of LSMO films and increase t_c for MIT. By minimizing these effects, an ultimate minimum $t_c = 3$ u.c. is achieved. However, the transport measurement indicates that dimensionally dependent localization effects prevent the thin films from exhibiting metallic behavior. These localization effects are induced by A-site disorder and/or oxygen vacancies that exist in these materials and amplified by the reduced dimensionality.

We thank Ziyang Meng for fruitful discussions. This paper was supported by U.S. Department of Energy (DOE) under Grant No. DOE DE-SC0002136. F.L and J.G are supported by NSFC Grant No. 11225422.

[1] C. H. Ahn, A. Bhattacharya, M. Di Ventra, J. N. Eckstein, C. D. Frisbie, M. E. Gershenson, A. M. Goldman, I. H. Inoue, J. Mannhart, A. J. Millis, A. F. Morpurgo, D. Natelson, and J.-M. Triscone, Electrostatic Modification of Novel Materials, Rev. Mod. Phys. **78**, 1185 (2006).

[2] R. G. Moore, J. D. Zhang, V. B. Nascimento, R. Jin, J. D. Guo, G. T. Wang, Z. Fang, D. Mandrus, and E. W. Plummer, A surface-tailored purely electronic Mott metal-to-insulator transition, Science **318**, 615 (2007).

[3] H. Y. Hwang, Y. Iwasa, M. Kawasaki, B. Keimer, N. Nagaosa, and Y. Tokura, Emergent phenomena at oxide interfaces, Nat. Mater. **11**, 103 (2012).

[4] D. G. Schlom, L.-Q. Chen, C.-B. Eom, K. M. Rabe, S. K. Streiffer, and J.-M. Triscone, Strain tuning of ferroelectric thin films, Annu. Rev. Mater. Res. **37**, 589 (2007).

[5] K. Yoshimatsu, T. Okabe, H. Kumigashira, S. Okamoto, S. Aizaki, A. Fujimori, and M. Oshima, Dimensional-Crossover-Driven Metal-Insulator Transition in $SrVO_3$ Ultrathin Films, Phys. Rev. Lett. **104**, 147601 (2010).

[6] A. V. Boris, Y. Matiks, E. Benckiser, A. Frano, P. Popovich, V. Hinkov, P. Wochner, M. Castro-Colin, E. Detemple, V. K. Malik, C. Bernhard, T. Prokscha, A. Suter, Z. Salman, E. Morenzoni, G. Cristiani, H.-U. Habermeier, and B. Keimer, Dimensionality control of electronic phase transitions in nickel-oxide superlattices, Science **332**, 937 (2011).

[7] A. Ohtomo and H. Y. Hwang, A high-mobility electron gas at the $LaAlO_3/SrTiO_3$ heterointerface, Nature (London) **427**, 423 (2004).

[8] N. Reyren, S. Thiel, A. D. Caviglia, L. F. Kourkoutis, G. Hammerl, C. Richter, C. W. Schneider, T. Kopp, A.-S. Rüetschi, D. Jaccard, M. Gabay, D. A. Muller, J.-M. Triscone, and J. Mannhart, Superconducting interfaces between insulating oxides, Science **317**, 1196 (2007).

[9] R. Scherwitzl, S. Gariglio, M. Gabay, P. Zubko, M. Gibert, and J.-M. Triscone, Metal-Insulator Transition in Ultrathin $LaNiO_3$ Films, Phys. Rev. Lett. **106**, 246403 (2011).

[10] P. D. C. King, H. I. Wei, Y. F. Nie, M. Uchida, C. Adamo, S. Zhu, X. He, I. Božović, D. G. Schlom, and K. M. Shen, Atomic-scale control of competing electronic phases in ultrathin $LaNiO_3$, Nat. Nanotechnol. **9**, 443 (2014).

[11] J. Xia, W. Siemons, G. Koster, M. R. Beasley, and A. Kapitulnik, Critical Thickness for Itinerant Ferromagnetism in Ultrathin Films of $SrRuO_3$, Phys. Rev. B **79**, 140407(R) (2009).

[12] J. Z. Sun, D. W. Abraham, R. A. Rao, and C. B. Eom, Thickness-dependent magnetotransport in ultrathin manganite films, Appl. Phys. Lett. **74**, 3017 (1999).

[13] R. P. Borges, W. Guichard, J. G. Lunney, J. M. D. Coey, and F. Ott, Magnetic and electric "dead" layers in $(La_{0.7}Sr_{0.3})MnO_3$ thin films, J. Appl. Phys. **89**, 3868 (2001).

[14] M. Angeloni, G. Balestrino, N. G. Boggio, P. G. Medaglia, P. Orgiani, and A. Tebano, Suppression of the metal-insulator transition temperature in thin $La_{0.7}Sr_{0.3}MnO_3$ films, J. Appl. Phys. **96**, 6387 (2004).

[15] A. Tebano, C. Aruta, P. G. Medaglia, F. Tozzi, G. Balestrino, A. A. Sidorenko, G. Allodi, R. De Renzi, G. Ghiringhelli, C. Dallera, L. Braicovich, and N. B. Brookes, Strain-Induced Phase Separation in $La_{0.7}Sr_{0.3}MnO_3$ Thin Films, Phys. Rev. B **74**, 245116 (2006).

[16] M. Huijben, L. W. Martin, Y.-H. Chu, M. B. Holcomb, P. Yu, G. Rijnders, D. H. A. Blank, and R. Ramesh, Critical Thickness and Orbital Ordering in Ultrathin $La_{0.7}Sr_{0.3}MnO_3$ Films, Phys. Rev. B **78**, 094413 (2008).

[17] A. Tebano, C. Aruta, S. Sanna, P. G. Medaglia, G. Balestrino, A. A. Sidorenko, R. De Renzi, G. Ghiringhelli, L. Braicovich, V. Bisogni, and N. B. Brookes, Evidence of Orbital Reconstruction at Interfaces in Ultrathin $La_{0.67}Sr_{0.33}MnO_3$ Films, Phys. Rev. Lett. **100**, 137401 (2008).

[18] B. J. Kim, D. Y. Kwon, T. Yajima, C. Bell, Y. Hikita, B. G. Kim, and H. Y. Hwang, Reentrant insulating state in ultrathin manganite films, Appl. Phys. Lett. **99**, 092513 (2011).

[19] L. Fitting Kourkoutis, J. H. Song, H. Y. Hwang, and D. A. Mullera, Microscopic origins for stabilizing room-temperature ferromagnetism in ultrathin manganite layers, Proc. Natl. Acad. Sci. USA **107**, 11682 (2010).

[20] Y. Tokura and Y. Tomioka, Colossal magnetoresistive manganites, J. Magn. Magn. Mater. **200**, 1 (1999).

[21] M. B. Lepetit, B. Mercey, and C. Simon, Interface Effects in Perovskite Thin Films, Phys. Rev. Lett. **108**, 087202 (2012).

[22] J. R. Sun, H. W. Yeung, H. K. Wong, T. Zhu, and B. G. Shen, Effects of vacuum annealing on the transport property of $La_{0.67}Sr_{0.33}MnO_{3-\delta}$ films, Eur. Phys. **35**, 481 (2003).

[23] G. Koster, B. L. Kropman, G. Rijnders, D. H. A. Blank, and H. Rogalla, Quasi-ideal strontium titanate crystal surfaces through formation of strontium hydroxide, Appl. Phys. Lett. **73**, 2920 (1998).

[24] A. Urushibara, Y. Moritomo, T. Arima, A. Asamitsu, G. Kido, and Y. Tokura, Insulator-Metal Transition and Giant Magnetoresistance in $La_{1-x}Sr_xMnO_3$, Phys. Rev. B **51**, 14103 (1995).

[25] H. Dulli, P. A. Dowben, S.-H. Liou, and E. W. Plummer, Surface Segregation and Restructuring of Colossal-Magnetoresistant Manganese Perovskites $La_{0.65}Sr_{0.35}MnO_3$, Phys. Rev. B **62**, R14629 (2000).

[26] A. Vailionis, H. Boschker, Z. Liao, J. R. A. Smit, G. Rijnders, M. Huijben, and G. Koster, Symmetry and lattice mismatch induced strain accommodation near and away from correlated perovskite interfaces, Appl. Phys. Lett. **105**, 131906 (2014).

[27] Z. Fang, I. V. Solovyev, and K. Terakura, Phase Diagram of Tetragonal Manganites, Phys. Rev. Lett. **84**, 3169 (2000).

[28] Y. Konishi, Z. Fang, M. Izumi, T. Manako, M. Kasai, H. Kuwahara, M. Kawasaki, K. Terakura, and Y. Tokura, Orbital-state-mediated phase-control of manganites, J. Phys. Soc. Jpn. **68**, 3790 (1999).

[29] G. Kresse and J. Furthmuller, Efficient iterative schemes for *ab initio* total-energy calculations using a plane-wave basis set, Phys. Rev. B **54**, 11169 (1996); G. Kresse and J. Hafner, *Ab initio* molecular dynamics for liquid metals, *ibid.* **47**, R558 (1993)

[30] P. E. Blochl, Projector Augmented-Wave Method, Phys. Rev. B **50**, 17953 (1994).

[31] J.P. Perdew, K. Burke, and M. Ernzerhof, Generalized Gradient Approximation Made Simple, Phys. Rev. Lett. **77**, 3865 (1996).

[32] J.-H. Park, E. Vescovo, H.-J. Kim, C. Kwon, R. Ramesh, and T. Venkatesan, Direct evidence for a half-metallic ferromagnet, Nature (London) **392**, 794 (1998).

[33] D. Pesquera, G. Herranz, A. Barla, E. Pellegrin, F. Bondino, E. Magnano, F. Sánchez, and J. Fontcuberta, Surface symmetry-breaking and strain effects on orbital occupancy in transition metal perovskite epitaxial films, Nat. Commun. **3**, 1189 (2012).

[34] P. A. Lee, and T. V. Ramakrishnan, Disordered Electronic Systems, Rev. Mod. Phys. **57**, 287 (1987).

[35] V. Dobrosavljevic, N. Trivedi, and J. M. Valles, Jr., in *Conductor Insulator Quantum Phase Transitions*, edited by V. Dobrosavljevic, N. Trivedi, and J. M. Valles, Jr. (Oxford University Press, Oxford, United Kingdom, 2012).

[36] S. Datta, *Electronic Transport in Mesoscopic Systems* (Cambridge University Press, Cambridge, United Kingdom, 1997).

[37] W. Brenig, G. H. Dohler, and H. Heyszenau, Hopping conductivity in highly anisotropic systems, Philos. Mag. **27**, 1093 (1973).